The effect of the conjugate-conduction parameter and Prandtl number on the free convective couple stress fluid flow over a vertical cylinder

Article *in* Progress in Computational Fluid Dynamics An International Journal · January 2014

DOI: 10.1504/PCFD.2014.064553

CITATIONS
0

READS
75

3 authors, including:

H. P. Rani
National Institute of Technology, Warangal
73 PUBLICATIONS **979** CITATIONS
SEE PROFILE

G. Janardhana Reddy
Central University of Karnataka
80 PUBLICATIONS **863** CITATIONS
SEE PROFILE

The effect of the conjugate-conduction parameter and Prandtl number on the free convective couple stress fluid flow over a vertical cylinder

H.P. Rani and G. Janardhana Reddy

Department of Mathematics,
National Institute of Technology,
Warangal-506004, AP, India
E-mail: hprani@nitw.ac.in
E-mail: janardhanreddy.nitw@gmail.com

Chang Nyung Kim*

Department of Mechanical Engineering,
College of Advanced Technology,
Industrial Liaison Research Institute,
Kyung Hee University,
Gyeonggi-do 446-701, Korea
Fax: +82-31-2029715
E-mail: cnkim@khu.ac.kr
*Corresponding author

Abstract: Numerical analysis is performed to study the conjugate heat transfer effects on the transient free convective couple stress fluid flow over a vertical slender hollow circular cylinder with the inner surface at a constant temperature. A set of non-dimensional governing equations namely, the continuity, momentum and energy equations is derived and these equations are unsteady non-linear and coupled. An unconditionally stable Crank-Nicolson type of implicit finite difference scheme is employed to obtain the discretised forms of governing equations. These equations are solved using the Thomas and pentadiagonal algorithms. The numerical results are compared and found to be in good agreement with previously published results as special cases of the present investigation. Transient velocity and temperature profiles, average skin-friction coefficient ($\overline{C_f}$) and average Nusselt number ($\overline{Nu}$) are shown graphically. In all these profiles it is observed that the time required for the variables to reach the steady-state increases with the increasing values of conjugate-conduction parameter (P) and Prandtl number. In the vicinity of the hot wall, the velocity and temperature of the fluid decrease as P increases. It is noticed that the steady-state values of $\overline{C_f}$ and $\overline{Nu}$ decreases as P increases.

Keywords: conjugate heat transfer; CHT; couple stress fluid; natural convection; vertical slender hollow cylinder; finite difference method.

Reference to this paper should be made as follows: Rani, H.P., Reddy, G.J. and Kim, C.N. (2014) 'The effect of the conjugate-conduction parameter and Prandtl number on the free convective couple stress fluid flow over a vertical cylinder', *Progress in Computational Fluid Dynamics*, Vol. 14, No. 5, pp.316–327.

Biographical notes: H.P. Rani is an Assistant Professor in Department of Mathematics, National Institute of Technology, Warangal, India. Her fields of interest are finite difference and volume methods in solving the problems related to heat and mass transfer.

G. Janardhana Reddy received his PhD from the Department of Mathematics at National Institute of Technology Warangal, India. His research interests include computational fluid dynamics, non-Newtonian fluids, heat and mass transfer problems.

Chang Nyung Kim is a Professor in Department of Mechanical Engineering, College of Engineering, Kyung Hee University, Korea. His research interests include fluid flow and heat and mass transfer.

1 Introduction

Unsteady natural convective flow of a viscous incompressible fluid is an important problem relevant to many engineering applications. The exact solution for this type of non-linear problems is still out of reach. Sparrow and Gregg (1956) provided the first approximate solution for the laminar buoyant flow of air bathing a vertical cylinder heated with a prescribed surface temperature, by applying the similarity method and power series expansion. Minkowycz and Sparrow (1974) obtained the solution for the same problem using the non-similarity method. While Fujii and Uehara (1970) analysed the local heat transfer results for arbitrary Prandtl numbers. Lee et al. (1988) investigated the similar problem along slender vertical cylinders and needles for the power-law variation in the wall temperature. In general, Bottemanne (1972) studied the combined effect of heat and mass transfer in the steady laminar boundary layer of a vertical cylinder for air and water vapour. Recently, Rani and Kim (2008) investigated the unsteady effects for the similar problem with temperature dependent viscosity. These types of problems have great importance in many physical situations such as the starting and shutting down of gas turbines, recuperative and regenerative heat exchangers and cooling passages in power reactors. In the glass and polymer industries, hot filaments, which are considered as a vertical cylinder, are cooled as they pass through the surrounding environment. In most of these situations, the temperature distribution in the fluid is mutually coupled to the temperature distribution in the solid body over which the fluid flows.

It can be observed that in the previous investigations the wall conduction resistance in the case of convective heat transfer between a solid cylinder wall and a fluid flow is generally neglected, i.e., the wall is assumed to be very thin and there is no conduction from the cylinder wall. But in many practical problems the information on the interfacial temperature is essential because the heat transfer characteristics are mainly determined by the temperature differences between the bulk flow and the interface. In order to take the account of physical reality, there has been a proclivity to move away from considering idealised mathematical problems in which the bounding wall is considered to be infinitesimally thin. Thus the conduction in solid wall and the convection in the fluid should be determined simultaneously. This type of convective heat transfer is referred to as a conjugate heat transfer (CHT) process and it arises due to the finite thickness of the wall. These type of problems have many practical applications, particularly those related to energy conservation in buildings, cold storage installations and cryogenic applications, such as medical and space technology and studied extensively (Gdalevich and Fertman, 1977; Miyamoto et al., 1980; Char et al., 1990; Pop and Na, 2000; Kaya, 2011).

These type of CHT problems have the growing importance in non-Newtonian fluids. They have application in modern technology and industries. Some important fields where couple stress fluids have applications includes squeezing and lubrication (Chu et al., 2006; Lin, 1998; Naduvinamani and Patilm 2009; Chang-Jian et al., 2010), bio-fluidmechanics (Srivastava, 1986, 2003), MHD flows and synthesis and plasticity of chemical compounds. Another interesting application was studied by Umavathi and Malashetty (1999) for the flow and heat transfer characteristics of Oberbeck convection of a couple stress fluid in a vertical porous stratum. Recently, Rani et al. (2011) obtained the numerical solution for the transient free convective couple stress fluid flow past a vertical cylinder. Stokes (1966) generalised the classical Newtonian model to include the effect of couple stresses in a way different from that of Eringen (1966). This is one among the several non-Newtonian fluid theories that are developed in the twentieth century. In his theory Stokes considered a body enclosing a volume without considering the microstructures of the infinitesimal fluid volume element. The set of all forces acting on an infinitesimal volume element is, in general, assumed to be equivalent to a single resultant force together with a resultant couple. The moment of the couple is assumed to be of non-zero value. With this assumption Stokes has proposed the theory of couple stress fluids allowing for the sustenance of couple stresses in addition to the usual stresses. Also, in his theory, curvature twist rate tensor is proposed based on the pure kinematic aspects of rotation vector and couple stress is defined in terms of this curvature twist rate tensor. Accordingly, in the balance of linear momentum of the couple stress flow model, fourth order derivatives of velocities are involved and, hence, separate angular momentum equation need not be considered. These fluids can also sustain the existence of body forces as usual and in addition by body couples as well. The stress tensor is no longer symmetric in this theory. This couple stress model has been widely used because of its great mathematical simplicity compared to that of the other models developed for the polar fluids. Recently, the study of couple stress fluid flows has been the subject of great interest, due to its widespread industrial and scientific applications as in the case of micropolar fluids.

From the previous studies, it can be noted that the CHT on the unsteady natural convective flow of a viscous incompressible couple stress fluid over a vertical cylinder has received very scant attention in the literature. Hence, in the present investigation our attention is focused on the conjugate problem of transient free convection over the outside surface of a vertical slender hollow cylinder immersed in a couple stress fluid. The temperature of the inner surface of the cylinder is kept at a constant value which is higher than the ambient fluid temperature and the temperature of the outer surface is determined by the conjugate solution of the steady-state energy equation of the solid and the boundary layer equations of the fluid flow. The governing equations are solved numerically by the implicit finite difference method to obtain the transient velocity and temperature profiles, coefficient of skin-friction and heat transfer rate for different values of conjugate-conduction parameter and Prandtl number.

In Section 2, a detailed description about the formulation of the problem is given. Also, the governing equations, such as mass, momentum and energy equations of an incompressible couple stress fluid flow past a vertical cylinder are derived and non-dimensionalised. In Section 3, the details about the grid generation and numerical methods for solving the above governing equations are given. In Section 4, transient two-dimensional velocity and temperature profiles, average skin-friction coefficient and heat transfer rate and comparison between couple stress fluid flow and Newtonian fluid flow are analysed. Finally, the concluding remarks are made in Section 5.

2 Formulation of the problem

A natural convective couple stress fluid flow past a vertical slender hollow cylinder of length l and outer radius r_0 ($l >> r_0$) is considered. The x-axis is measured vertically upward along the axis of the cylinder. The origin of x is taken to be at the leading edge of the cylinder, where the boundary layer thickness is zero. The radial coordinate, r, is measured perpendicular to the axis of the cylinder. Assume that the fluid have constant physical properties and the fluid flow is unsteady, laminar and two-dimensional. The surrounding stationary fluid temperature is assumed to be of ambient temperature (${T_\infty}'$). The temperature of the inside surface of the cylinder is maintained at a constant temperature of ${T_0}'$, where ${T_0}' > {T_\infty}'$. Initially, i.e., at time $t' = 0$ it is assumed that the outer surface of the cylinder and the fluid are of the same temperature ${T_\infty}'$. As time increases ($t' > 0$), the temperature of the outer surface of the cylinder is raised to the solid-fluid interface temperature ${T_w}'$ and maintained at the same level for all time $t' > 0$. This temperature ${T_w}'$ is determined by the conjugate solution of the steady-state energy equation of the solid and the boundary layer equations of the fluid flow and is discussed elsewhere. Due to this temperature difference between the outer surface of the cylinder and surrounding fluid, there occurs a density difference which interacts with the gravitational force and hence there occurs a natural convection flow (Boussinesq's approximation). It is assumed that the effect of viscous dissipation is negligible in the energy equation. Under these assumptions, the boundary layer equations of mass, momentum and energy with Boussinesq's approximation are as follows:

$$\frac{\partial (ru)}{\partial x} + \frac{\partial (rv)}{\partial r} = 0 \tag{1}$$

$$\begin{aligned} &\rho\left(\frac{\partial u}{\partial t'} + u\frac{\partial u}{\partial x} + v\frac{\partial u}{\partial r}\right) \\ &= \rho g\beta\left(T' - {T_\infty}'\right) + \frac{\mu}{r}\frac{\partial}{\partial r}\left(r\frac{\partial u}{\partial r}\right) \\ &\quad - \eta\nabla^4 u \end{aligned} \tag{2}$$

$$\frac{\partial T'}{\partial t'} + u\frac{\partial T'}{\partial x} + v\frac{\partial T'}{\partial r} = \frac{\alpha}{r}\frac{\partial}{\partial r}\left(r\frac{\partial T'}{\partial r}\right) \tag{3}$$

where η is a material constant with the dimension of momentum and describes the couple stress fluid property. Usually, the ratio of material constants η and μ has the dimensions of length square, i.e., r_0^2 (see Stokes, 1984).

Stokes (1984) proposed mainly two types of boundary conditions, namely, the vorticity of the fluid on the boundary is equal to the rotational velocity of the boundary and the couple stresses vanish on the boundary. The present problem is solved based on the former boundary condition. In view of this, the relevant initial and boundary conditions are given by:

$$\begin{aligned} &t' = 0\colon u = 0, v = 0, T' = {T_\infty}' && \text{for all } x \text{ and } r \\ &t' > 0\colon u = 0, v = 0, T' = {T_w}' && \text{at } r = r_0 \\ &\qquad u = 0, v = 0, T' = {T_\infty}' && \text{at } x = 0 \\ &\qquad u \to 0, v \to 0, T' \to {T_\infty}' && \text{as } r \to \infty \end{aligned} \tag{4}$$

and,

$$\frac{\partial u}{\partial r} = \frac{\partial v}{\partial x} \qquad \text{at } r = r_0 \text{ and as } r \to \infty \tag{5}$$

In the above equation (4), ${T_w}'$ represents the unknown solid-fluid interface temperature and is determined as follows:

The governing equation for the temperature distribution within the slender hollow circular cylinder, based on the simplification that the wall of cylinder constantly transfers its heat to the surrounding fluid, is given by (Chang, 2006)

$$\frac{\partial^2 {T_s}'}{\partial r^2} + \frac{1}{r}\frac{\partial {T_s}'}{\partial r} = 0; \qquad 0 \le x \le l; \qquad r_i \le r \le r_0 \tag{6}$$

subject to

$$\begin{aligned} {T_s}' &= {T_0}' \quad \text{at} \quad r = r_i \\ {T_s}' &= {T_w}' = T'(x, r_0) \quad \text{at} \quad r = r_0 \end{aligned} \tag{7}$$

The axial conduction term in the heat conduction equation (6) of the cylinder can be omitted according to Chang (2006), since the outer radius of the hollow cylinder, r_0, is assumed to be small compared to its length, l.

The general solution of equation (6) along with equation (7) is given by

$${T_s}' = {T_0}' + (T'(x, r_0) - {T_0}')\frac{\ln(r/r_i)}{\ln(r_0/r_i)} \tag{8}$$

On the other hand, equation (6) is coupled with the energy equation in the fluid region based on the condition that the temperature and the heat flux are continuous at the solid-fluid interface, namely

$$\begin{aligned} &{T_s}' = T'(x, r_0), \\ &-k_s\frac{\partial {T_s}'}{\partial r} = -k_f\frac{\partial T'(x, r_0)}{\partial r} \\ &\text{on } r = r_0 \end{aligned} \tag{9}$$

Using equations (8) and (9), the temperature distribution ${T_w}'$ at the interface is given by

$$\begin{aligned} {T_w}' &= T'(x, r_0) \\ &= r_0\frac{k_f}{k_s}\ln\left(\frac{r_0}{r_i}\right)\frac{\partial T'(x, r_0)}{\partial r} + {T_0}' \\ &\quad \text{at} \quad r = r_0 \end{aligned} \tag{10}$$

In the process of the non-dimensionalisation of equations (1) to (3), a length scale of $\left(\frac{\eta}{\mu}\right)^{\frac{1}{2}}$ is observed. In order to simplify the formulation of the current problem the value of $\left(\frac{\eta}{\mu}\right)^{\frac{1}{2}}$ is set to the outer radii, r_0, of the hollow cylinder.

By introducing the following non-dimensional quantities

$$X = Gr^{-1}\frac{x}{r_0}, \quad R = \frac{r}{r_0}, \quad U = Gr^{-1}\frac{ur_0}{\nu}, \quad V = \frac{vr_0}{\nu}, \quad t = \frac{\nu t'}{r_0^2}, \tag{11}$$

$$T = \frac{T' - T_\infty{}'}{T_0{}' - T_\infty{}'}, \quad Gr = \frac{g\beta r_0^3\left(T_0{}' - T_\infty{}'\right)}{\nu^2}, \quad Pr = \frac{\nu}{\alpha}, \quad P = \frac{k_f}{k_s}\ln\left(\frac{r_0}{r_i}\right)$$

(the symbols are explained in the nomenclature) in equations (1) to (3), they reduced to the following form:

$$\frac{\partial U}{\partial X} + \frac{\partial V}{\partial R} + \frac{V}{R} = 0 \tag{12}$$

$$\frac{\partial U}{\partial t} + U\frac{\partial U}{\partial X} + V\frac{\partial U}{\partial R} = T + \frac{\partial U}{\partial R}\left(\frac{1}{R} - \frac{1}{R^3}\right) + \frac{\partial^2 U}{\partial R^2}\left(1 + \frac{1}{R^2}\right) - \frac{2}{R}\frac{\partial^3 U}{\partial R^3} - \frac{\partial^4 U}{\partial R^4} \tag{13}$$

$$\frac{\partial T}{\partial t} + U\frac{\partial T}{\partial X} + V\frac{\partial T}{\partial R} = \frac{1}{Pr}\left(\frac{\partial^2 T}{\partial R^2} + \frac{1}{R}\frac{\partial T}{\partial R}\right) \tag{14}$$

The corresponding initial and boundary conditions in non-dimensional quantities are given by

$$\begin{aligned} &t = 0\colon U = 0, V = 0, T = 0 && \text{for all } X \text{ and } R \\ &t > 0\colon U = 0, V = 0, \\ &\quad T - 1 = P\tfrac{\partial T}{\partial R} && \text{at } R = 1 \\ &\quad U = 0, V = 0, T = 0 && \text{at } X = 0 \\ &\quad U \to 0, V \to 0, T \to 0 && \text{as } R \to \infty \end{aligned} \tag{15}$$

Similarly, equation (5) can be changed into the following non-dimensional form

$$\frac{\partial U}{\partial R} = \frac{1}{Gr^2}\frac{\partial V}{\partial X} \qquad \text{at } R = 1 \text{ and as } R \to \infty \tag{16}$$

3 Numerical solution of the problem

In order to solve the unsteady coupled non-linear governing equations (12) to (14) an implicit finite difference scheme of Crank-Nicolson type has been employed. The finite difference equations corresponding to equations (12) to (14) are as follows:

$$\begin{aligned} &\frac{U_{i,j}^{k+1} - U_{i-1,j}^{k+1} + U_{i,j}^{k} - U_{i-1,j}^{k}}{\Delta X} \\ &+ \frac{V_{i,j+1}^{k+1} - V_{i,j-1}^{k+1} + V_{i,j+1}^{k} - V_{i,j-1}^{k}}{2\Delta R} \\ &+ \frac{V_{i,j}^{k+1} + V_{i,j}^{k}}{[1 + (j-1)\Delta R]} = 0 \end{aligned} \tag{17}$$

$$\begin{aligned} &\frac{U_{i,j}^{k+1} - U_{i,j}^{k}}{\Delta t} + \frac{U_{i,j}^{k}}{2\Delta X}\left(U_{i,j}^{k+1} - U_{i-1,j}^{k+1} + U_{i,j}^{k} - U_{i-1,j}^{k}\right) \\ &+ \frac{V_{i,j}^{k}}{4\Delta R}\left(U_{i,j+1}^{k+1} - U_{i,j-1}^{k+1} + U_{i,j+1}^{k} - U_{i,j-1}^{k}\right) \\ &= \frac{T_{i,j}^{k+1} + T_{i,j}^{k}}{2} + \left(\frac{U_{i,j+1}^{k+1} - U_{i,j-1}^{k+1} + U_{i,j+1}^{k} - U_{i,j-1}^{k}}{4[1 + (j-1)\Delta R]\Delta R}\right) \\ &+ \left(\frac{U_{i,j-1}^{k+1} - 2U_{i,j}^{k+1} + U_{i,j+1}^{k+1} + U_{i,j-1}^{k} - 2U_{i,j}^{k} + U_{i,j+1}^{k}}{2(\Delta R)^2}\right) \\ &- \left(\frac{U_{i,j+2}^{k+1} - 4U_{i,j+1}^{k+1} + 6U_{i,j}^{k+1} - 4U_{i,j-1}^{k+1} + U_{i,j-2}^{k+1} + U_{i,j+2}^{k} - 4U_{i,j+1}^{k} + 6U_{i,j}^{k} - 4U_{i,j-1}^{k} + U_{i,j-2}^{k}}{2(\Delta R)^4}\right) \\ &- \left(\frac{U_{i,j+2}^{k+1} - 2U_{i,j+1}^{k+1} + 2U_{i,j-1}^{k+1} - U_{i,j-2}^{k+1} + U_{i,j+2}^{k} - 2U_{i,j+1}^{k} + 2U_{i,j-1}^{k} - U_{i,j-2}^{k}}{2[1 + (j-1)\Delta R](\Delta R)^3}\right) \\ &+ \left(\frac{U_{i,j-1}^{k+1} - 2U_{i,j}^{k+1} + U_{i,j+1}^{k+1} + U_{i,j-1}^{k} - 2U_{i,j}^{k} + U_{i,j+1}^{k}}{2[1 + (j-1)\Delta R]^2(\Delta R)^2}\right) \\ &- \left(\frac{U_{i,j+1}^{k+1} - U_{i,j-1}^{k+1} + U_{i,j+1}^{k} - U_{i,j-1}^{k}}{4[1 + (j-1)\Delta R]^3\Delta R}\right) \end{aligned} \tag{18}$$

$$\begin{aligned} &\frac{T_{i,j}^{k+1} - T_{i,j}^{k}}{\Delta t} + \frac{U_{i,j}^{k}}{2\Delta X}\left(T_{i,j}^{k+1} - T_{i-1,j}^{k+1} + T_{i,j}^{k} - T_{i-1,j}^{k}\right) \\ &+ \frac{V_{i,j}^{k}}{4\Delta R}\left(T_{i,j+1}^{k+1} - T_{i,j-1}^{k+1} + T_{i,j+1}^{k} - T_{i,j-1}^{k}\right) \\ &= \left(\frac{T_{i,j-1}^{k+1} - 2T_{i,j}^{k+1} + T_{i,j+1}^{k+1} + T_{i,j-1}^{k} - 2T_{i,j}^{k} + T_{i,j+1}^{k}}{2Pr(\Delta R)^2}\right) \\ &+ \left(\frac{T_{i,j+1}^{k+1} - T_{i,j-1}^{k+1} + T_{i,j+1}^{k} - T_{i,j-1}^{k}}{4Pr[1 + (j-1)\Delta R]\Delta R}\right) \end{aligned} \tag{19}$$

To solve these equations, the region of integration is considered as a rectangle composed of the lines indicating $X_{min} = 0$, $X_{max} = 1$, $R_{min} = 1$ and $R_{max} = 20$, where R_{max} corresponds to $R = \infty$ which lies very far

from the momentum and energy boundary layers. In the above equations (17) to (19) the subscripts i and j designate the grid points along the X and R coordinates, respectively, where $X = i\Delta X$ and $R = 1 + (j-1)\Delta R$ and the superscript k implies the time step along the time t, where $t = k\Delta t$, with ΔX, ΔR and Δt denoting the mesh size in the X, R coordinates and along time t, respectively. In order to obtain an economical and reliable grid system for the computations, a grid independency test has been performed. The steady-state velocity and temperature values obtained with the grid system of 100×500 differ in the second decimal place from those with the grid system of 50×250, and differ in the fifth decimal place from those with the grid system of $200 \times 1,000$. Hence, the grid system of 100×500 has been selected for all subsequent analyses, with the mesh sizes in X and R directions taken as 0.01 and 0.03, respectively. Also, the time step size dependency has been tested from which Δt = 0.01 yielded a reliable result.

From the initial conditions given in equation (15), the values of velocity U, V and temperature T are known at time $t = 0$, then the values of T, U and V at the next time step can be calculated by equations (12) to (14) using the boundary conditions given in equations (15) and (16). Generally, when the above variables are known at $t = k\Delta t$, the variables at $t = (k+1)\Delta t$ are calculated as follows. The finite difference equations (18) and (19) at every internal nodal point on a particular i-level constitute a tridiagonal and pentadiagonal system of equations. Such a system of equations is solved by the pentadiagonal algorithm (Rosenberg, 1969) and Thomas algorithm (Carnahan et al., 1969). At first, the temperature T is calculated from equation (19) at every j nodal point on a particular i-level at the $(k+1)^{\text{th}}$ time step. By making use of these known values of T, the velocity U at the $(k+1)^{\text{th}}$ time step is calculated from equation (18) in a similar manner. Thus, the values of T and U are known at a particular i-level. Then, the velocity V is calculated from equation (17) explicitly. This process is repeated for the consecutive i-levels with many times of sweeping until the convergence; thus the values of T, U and V are known at all grid points in the rectangular region at the $(k+1)^{\text{th}}$ time step. This iterative procedure is repeated for many time steps until the steady-state solution is reached. The steady-state solution is assumed to have been reached when the absolute difference between the values of velocity as well as temperature at two consecutive time steps is less than 10^{-5} at all grid points. The truncation error in the employed finite difference approximation is $O(\Delta t^2 + \Delta R^2 + \Delta X)$ and tends to zero as ΔX, ΔR and $\Delta t \to 0$. Hence the system is compatible. Also, this finite difference scheme is unconditionally stable and therefore, stability and compatibility ensure the convergence.

4 Results and discussion

For the validation, the steady-state velocity and temperature profiles in the case of Newtonian fluids are compared with the existing numerical results of Lee et al. (1988) for Pr = 0.7 and $P = 0.0$, as there are no experimental or analytical studies available. The current results are found to be in good agreement with the previous results as shown in Figure 1.

Figure 1 Comparison of the velocity and temperature profiles for Newtonian fluids

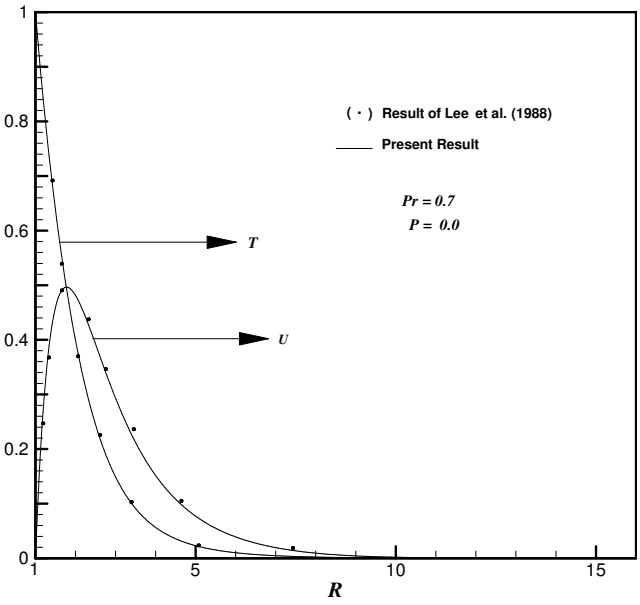

The simulated results are presented to outline the general physics involved in the effects of different Pr (= 0.71, 1.0, 2.0 and 3.0) and P (= 0.1, 0.5, 1.0 and 2.0) on the transient velocity and temperature profiles. The simulated transient behaviour of the dimensionless velocity, temperature, average skin-friction coefficient and heat transfer rate are discussed in detail in the succeeding subsections.

4.1 Velocity

The simulated transient velocities (U) at point (X, R) = (1, 3.47) for different values of Pr and conjugate-conduction parameter P against t is shown graphically in Figure 2. Figure 2(a) shows the variation of Pr with fixed P = 0.5 and Figure 2(b) for the variation of P with fixed Pr = 0.71. From Figures 2(a) and 2(b) it is observed that the velocities increase with time monotonically from zero and reach temporal maxima, then decrease and at last reach the asymptotic steady-state. For

example, in Figure 2(a) when Pr = 0.71, the velocity increases with time monotonically from zero and reaches the temporal maximum, then slightly decreases with time and becomes asymptotically steady. It is observed that at the very early time (i.e., $t << 1$), the heat transfer is dominated by conduction. Shortly later, there exists a period when the heat transfer rate is influenced by the effect of convection with increasing upward velocities along the time. When this transient period is almost ending and just before the steady-state is about to be reached, there exist overshoots of the velocities. From Figures 3(a) and 3(b) it can be observed that velocity profiles reach their maximum value approximately at point (X, R) = (1, 3.47). Similarly, the velocities at other locations also exhibit somewhat similar transient behaviour. As noted in Figure 2(a), the magnitude of this overshoot of the velocities decreases as Pr is increased, since with the increasing Pr the velocity diffusion is increased [refer equation (13)]. Hence, there is a less resistance to the fluid flow in the region of the temporal maximum of velocity. The time needed to reach the temporal maximum of the velocity increases as Pr increases. It is also noticed that for small values of Pr the temporal maximum is reached at early times. For all values of P, Figure 2(b reveals that it has the same trend as the variation of velocity with respect to Pr as shown in Figure 2(a), but the temporal maximum is attained at an early state. In association with the transient characteristics of the velocity, similar trends of the temperature fluctuation can be observed and will be described in Figure 4.

Figure 3 shows the simulated steady-state velocity profiles against the R at X = 1.0 for different values of Pr and P. Figure 3(a) shows the variation of Pr with fixed P = 0.5 and Figure 3(b) for the variation of P with fixed Pr = 0.71. From these figures it is observed that the velocity profiles start with the value zero at the wall, reach their maxima and then monotonically decrease to zero along the radial coordinate. Also it is observed that in the vicinity of the wall the magnitude of the axial velocity is rapidly increasing as R increases from R_{min} (=1). Time required to reach the steady-state increases as Pr and P increases. From Figure 3(a) it is observed that the velocity decreases with increasing values of Pr because the thermal convection is confined to a region which is near the wall for higher values of Pr [refer to Figure 5(a)]. Thus the radial position for the peak axial velocity moves toward the wall as Pr is increased. From Figure 3(b) it is observed that the effect of lower wall conductance (k_s) or higher convective cooling effect due to greater k_f increases the value of P and decreases the velocity in the vicinity of the hot wall, i.e., in the region $1 \leq R \leq 7.59$. While the opposite trend is observed in the edge of the boundary layer region, i.e., increasing values of P leads to the higher values of velocity therein because of an enhanced thermal transport due to higher thermal conductivity of the fluid.

Figure 2 The simulated transient velocity at (1, 3.47) for (a) variation of Pr and (b) variation of P

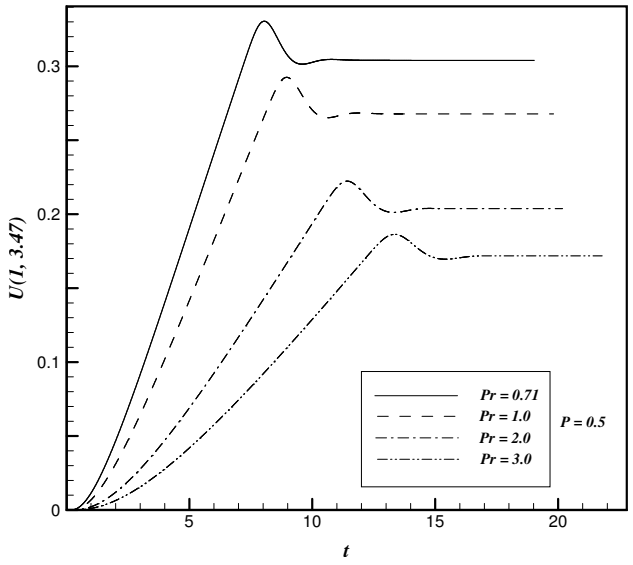

(a)

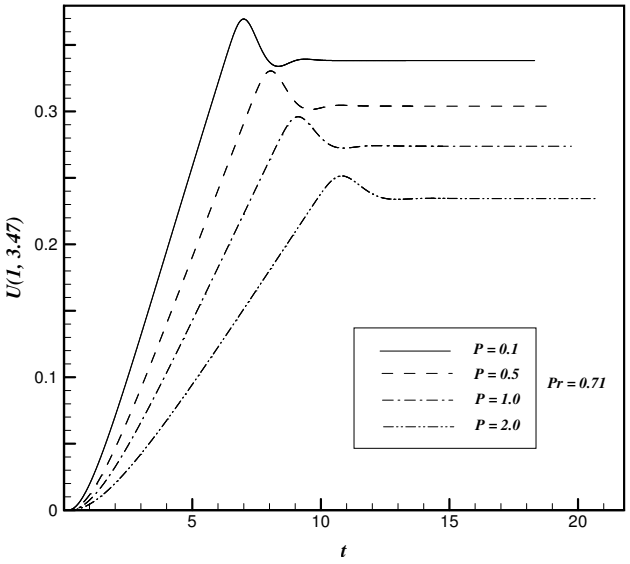

(b)

4.2 Temperature

The simulated transient temperatures (T) for different values of Pr and P with respect to t is shown at the point (1, 1.15) in Figure 4. Figure 4(a) shows the variation of Pr with fixed P = 0.5 and Figure 4(b) for the variation of P with fixed Pr = 0.71. From Figures 4(a) and 4(b) it is observed that these profiles increase with time, reach a temporal maxima, decrease and again after a slight increase attain the steady-state asymptotically. The temperatures at other locations also exhibit somewhat similar transient behaviour. During the initial period, the nature of the transient temperature profiles is particularly noticeable. From Figure 4(a) it is observed that for small value of Pr (= 0.71), the transient temperature profiles initially coincide and then deviate from each other after some time. Also, the time required to reach the temporal maximum of the temperature increases with increasing values of Pr. It

can be noticed that for small values of Pr the temporal maximum is attained at an early times. Here, it is observed that the maximum temperature value decreases with the increasing Pr. Figure 4(b) shows that it has the same trend as the variation of temperature with respect to Pr as shown in Figure 4(a), but the temporal maximum is reached at an early state for all values of P. From Figures 4(a) and 4(b) it is noticed that during the initial time, the variation of temperature with P is observed to be larger than that with Pr. This result implies that the temperature field is more strongly affected by the conjugate-conduction parameter, since an increased value of P corresponds to a lower wall conductance k_s and promotes greater surface temperature variations as shown in Figure 4(b).

Figure 3 The simulated steady-state velocity profile at $X = 1.0$ for (a) variation of Pr and (b) variation of P

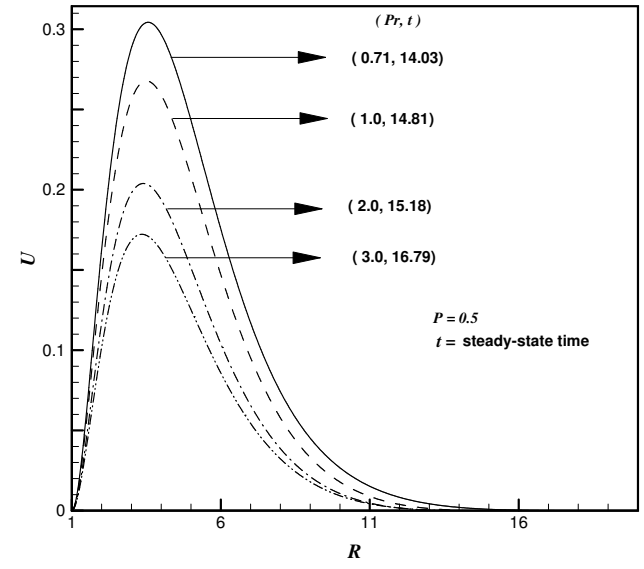

(a)

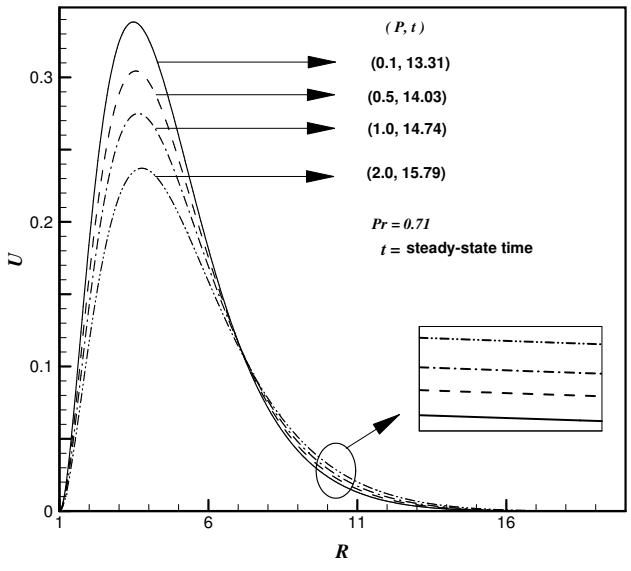

(b)

Figure 4 The simulated transient temperature at (1, 1.15) for (a) variation of Pr and (b) variation of P

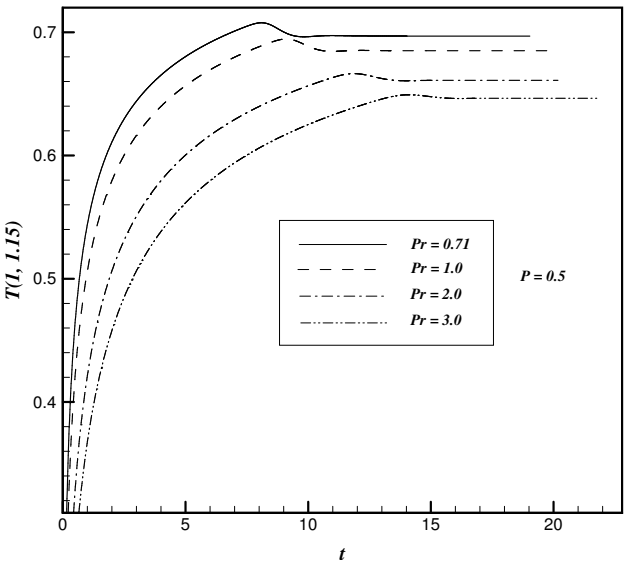

(a)

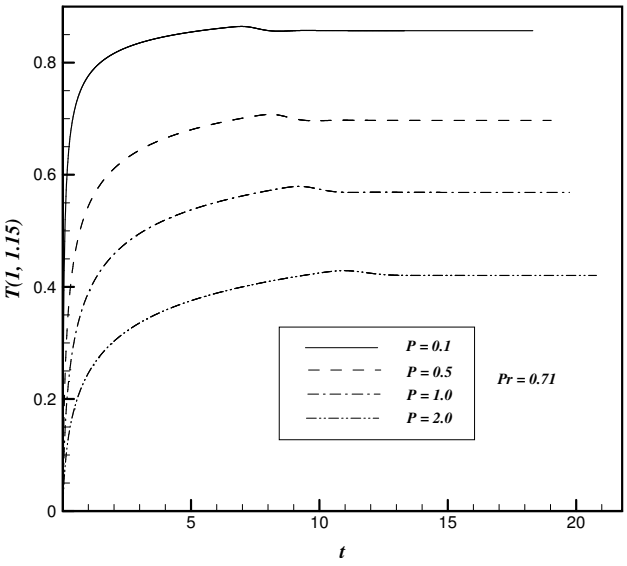

(b)

The simulated steady-state temperature profiles for different values of Pr and P at $X = 1.0$ against the R are shown in Figure 5. Figure 5(a) depicts the variation of Pr with fixed $P = 0.5$ and Figure 5b for the variation of P with fixed $Pr = 0.71$. From these figures it is observed that the temperature profiles start with the hot wall temperature and then monotonically decrease to zero along the radial coordinate. As mentioned before, as Pr is increased the thickness of the thermal boundary layer is decreased with an increased temperature gradient near the wall, which moves the radial position for the peak axial velocity toward the wall. Also, the time needed for the temperature to reach the steady-state increases as Pr and P increases. From Figure 5(a) it is observed that the steady temperature value decreases with increasing values of Pr for fixed P. Larger Pr values give rise to thinner thermal boundary layer, since

a larger Pr value means that the thermal diffusion from the wall is not prevailing while the velocity diffusion is noticeable even away from the wall. Figure 5(b) reveals that it has the same trend as the variation of velocity with respect to P as shown in Figure 3(b), i.e., in the vicinity of the hot wall the steady temperature value decreases as the conjugate-conduction parameter P increases. This is due to the reason that the temperature at the solid-fluid interface is reduced since the temperature at the inner surface of the cylinder is kept constant. As a result the temperature profiles as well as the velocity profiles shifts downwards in the fluid.

Figure 5 The simulated steady-state temperature profile at X = 1.0 for (a) variation of Pr and (b) variation of P

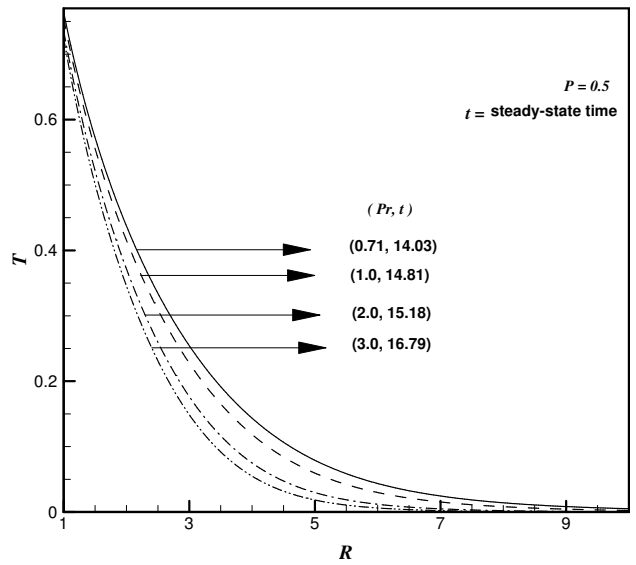

(a)

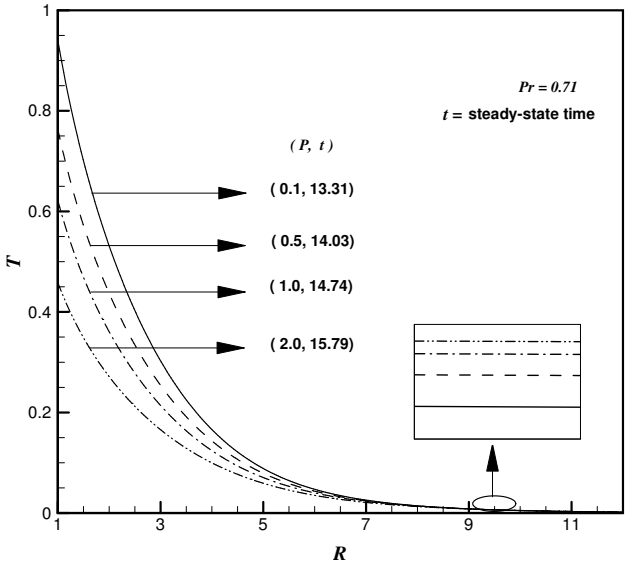

(b)

4.3 Average skin-friction coefficient and heat transfer rate

Knowing the unsteady behaviour of velocity and temperature profiles, it is worth to study the average skin-friction coefficient and the average heat transfer rate (Nusselt number). The friction coefficient is an important parameter in the heat transfer studies since it is directly related to the heat transfer coefficient. Increased skin-friction is generally a disadvantage in technical applications, while the increased heat transfer can be exploited in some applications such as heat exchangers, but should be avoided in others such as gas turbine applications, for instance. For the present problem these skin-friction coefficient and heat transfer rate are derived and given in the following equations:

The wall shear stress at the wall can be expressed as $\tau_w = \left(\mu \frac{\partial u}{\partial r}\right)_{r=r_0}$. Considering $\frac{\mu^2 Gr}{\rho r_0^2}$ to be the characteristic shear stress, then the non-dimensional local skin-friction coefficient can be written as

$$C_f = \left(\frac{\partial U}{\partial R}\right)_{R=1} \tag{20}$$

The integration of the equation (20) from X = 0 to X = 1 gives the following average skin-friction coefficient.

$$\overline{C_f} = \int_0^1 \left(\frac{\partial U}{\partial R}\right)_{R=1} dX \tag{21}$$

The local Nusselt number is given by $Nu_x = \frac{\dot{q_w} r_0}{k_f (T_0' - T_\infty')}$, where the heat transfer, $\dot{q_w} = -k_f \left(\frac{\partial T'}{\partial r}\right)_{r=r_0}$. In non-dimensional form it can be written as

$$Nu_X = -\left(\frac{\partial T}{\partial R}\right)_{R=1} \tag{22}$$

The integration of the above equation (22) with respect to X from 0 to 1 yields the following average Nusselt number.

$$\overline{Nu} = -\int_0^1 \left(\frac{\partial T}{\partial R}\right)_{R=1} dX \tag{23}$$

The derivatives involved in equations (21) and (23) are evaluated by using a five-point approximation formula and then the integrals are evaluated by using the Newton-Cotes closed integration formula. The simulated average non-dimensional skin-friction and heat transfer coefficients have been plotted against the time in Figures 6 and 7 for different values of Pr and P.

Figure 6 The simulated average skin-friction for (a) variation of Pr and (b) variation of P

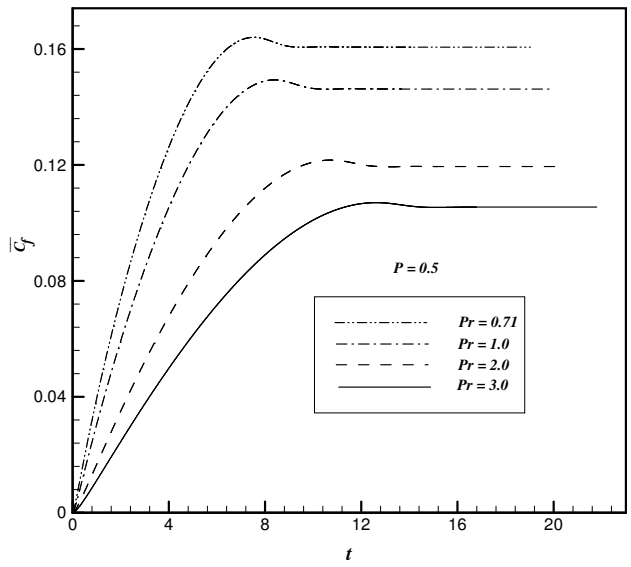

(a)

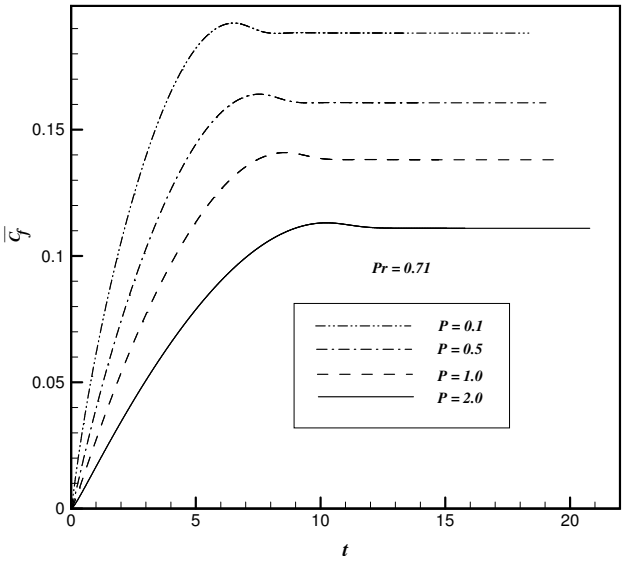

(b)

The effects of Pr and P on the simulated average skin-friction coefficient are shown in Figures 6(a) and 6(b), respectively. From Figures 6(a) and 6(b) it is observed that for all values of Pr and P the average skin-friction coefficients increase at first with time, attain the peak values and, after slight decrease, reach asymptotically steady-state. Because the buoyancy-induced flow velocity is relatively low at the initial transient period, as seen in Figure 2, the wall shear stress remain small, as shown in Figure 6. However, the wall shear stress increases as the time proceeds, yielding an increase in the skin-friction coefficient. It is also observed from Figure 6(a) that for increasing values of Pr the average skin-friction coefficient decreases. This result lies in the same line with the velocity profiles plotted in Figure 3(a). From Figure 6(b) it is observed that the average skin-friction coefficient decreases as P increases. It is related to the fact that the increased value of P decreases the velocity of the fluid within the boundary layer, as mentioned in Figure 3(b). It is also noticed that from Figures 6(a) and 6(b), during the initial period, the effect of P on the dimensionless skin-friction coefficient is considerable, though this effect is not so stronger as the influence of Pr on the same variable. This result means that the average skin-friction coefficient is more strongly affected by P compared to Pr.

Figure 7 The simulated average Nusselt number for (a) variation of Pr and (b) variation of P

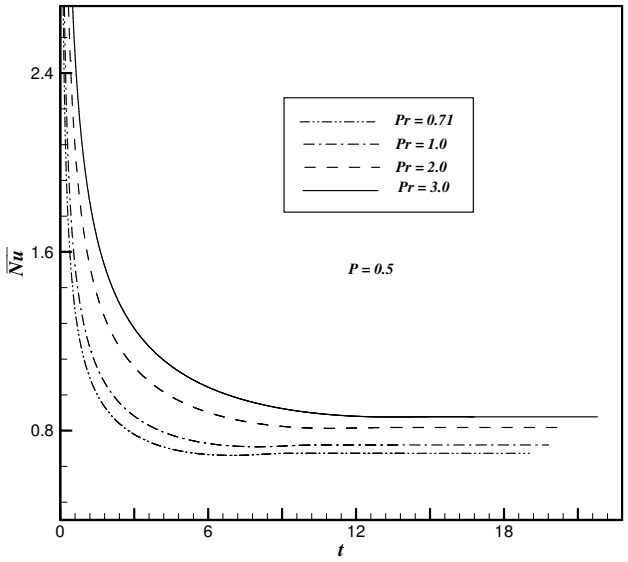

(a)

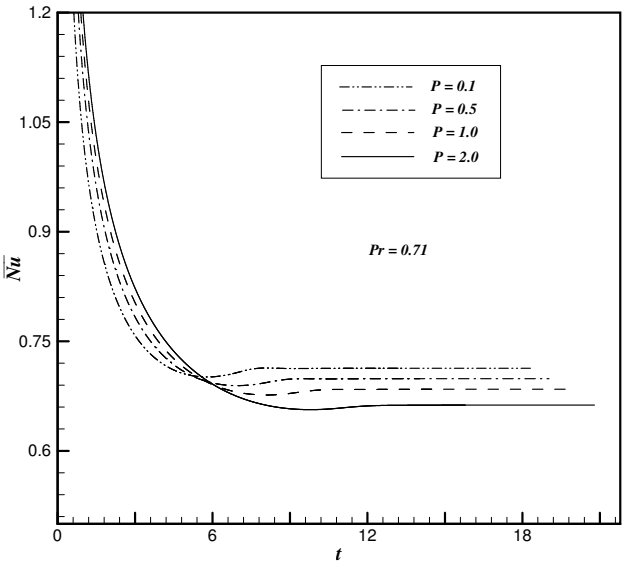

(b)

Table 1 The times needed for different variables to reach the temporal maxima and the steady-state and the maximum velocities with different Pr and P values for (a) couple stress fluid and (b) Newtonian fluid

Pr	*P*	*Temporal maximum (t) of*		*Steady-state time (t)*	*Maximum velocity (U) at X = 1.0*
		U	*T*		
			(a)		
0.71	0.1	7.05	6.99	13.34	0.3384
0.71	0.5	8.09	8.11	14.06	0.3045
0.71	1.0	9.14	9.24	14.78	0.2750
0.71	2.0	10.85	10.99	15.79	0.2374
1.0	0.5	8.99	9.14	14.85	0.2679
2.0	0.5	11.45	11.88	15.19	0.2039
3.0	0.5	13.39	14.12	16.79	0.1724
			(b)		
0.71	0.1	4.96	4.69	13.99	0.4709
0.71	0.5	6.05	5.78	14.88	0.4015
0.71	1.0	7.09	6.84	15.69	0.3494
0.71	2.0	8.69	8.39	16.78	0.2894
1.0	0.5	6.28	6.08	14.56	0.3786
2.0	0.5	7.07	6.89	14.00	0.3243
3.0	0.5	7.69	7.56	13.96	0.2898

In Figures 7(a) and 7(b) the effects of Pr and P on the simulated average heat transfer rate are shown, respectively. From Figures 7(a) and 7(b) it is observed that for short period of time after $t = 0$, the average Nusselt numbers are almost the same for all values of Pr and P. This shows that initially heat conduction is dominating compared with heat convection. Figure 7a reveals that an increase in the value of Pr leads to a increase in the values of the average heat transfer rate. Increasing Pr speeds up the spatial decay of the temperature near the heated surface together with increased flow velocity near the wall, yielding an increase in the rate of heat transfer. From Figure 7(b) it is observed that with the increasing values of P, i.e., with lower wall conductance (k_s), initially, $t \leq 5.59$, the average heat transfer rate is almost same with increasing trend. Later it decreases with increasing values of P and attains the steady-state.

4.4 Comparison between the couple stress fluids and Newtonian fluids

Table 1 explains the variation of couple stress fluid flow from Newtonian fluid flow in terms of the time for the flow variables U and T to reach the temporal maximum and the steady-state with different Pr and P values, where Table 1(a) tabulates the values for couple stress fluid and Table 1(b) for Newtonian fluid. Table 1(a) shows that the times required for all the flow variables to reach the temporal maxima and steady-state increase with increasing values of Pr and P. Also, from Tables 1(a) and 1(b), we can see that with all values of Pr and P the times for all the flow variables to reach the temporal maxima for the couple stress fluid are larger than those for the Newtonian fluid. It is also noticed that with increasing values of P, the times required for all the flow variables to reach the steady-state for the couple stress fluid are rather smaller than those for the Newtonian fluid, which means that the transient periods after the temporal maxima are quite longer for the Newtonian fluid compared to those for the couple stress fluid. While the opposite trend is observed for Pr. Also, for all values of Pr and P it is observed that maximum velocity occurs at $X = 1.0$ of a couple stress fluid is decreased compared with that of Newtonian fluid.

Table 2 Simulated average skin-friction coefficient ($\overline{C_f}$) and Nusselt number ($\overline{Nu}$) in steady-state with different Pr and P values for (a) couple stress fluid and (b) Newtonian fluid.

Pr	*P*	$\overline{C_f}$	$\overline{Nu}$
		(a)	
0.71	0.1	0.1884	0.7134
0.71	0.5	0.1608	0.6989
0.71	1.0	0.1382	0.6846
0.71	2.0	0.1110	0.6629
1.0	0.5	0.1464	0.7359
2.0	0.5	0.1198	0.8144
3.0	0.5	0.1055	0.8625
		(b)	
0.71	0.1	1.3108	1.0878
0.71	0.5	1.0484	1.0494
0.71	1.0	0.8659	1.0113
0.71	2.0	0.6716	0.9587
1.0	0.5	1.0034	1.0933
2.0	0.5	0.8935	1.2109
3.0	0.5	0.8209	1.2979

Table 2 demonstrates the comparison between couple stress fluid to Newtonian fluid in terms of average skin-friction coefficient and average heat transfer rate with different values of Pr and P, where Table 2(a) shows the values for couple stress fluid and Table 2(b) for Newtonian fluid. From Tables 2(a) and 2(b), it is observed that the average

values of skin-friction coefficient and Nusselt number of a couple stress fluid is smaller than that of the Newtonian fluid for all values of Pr and P. In summary, Table 2 reveals that the characteristics of skin-friction and heat transfer of a couple stress fluid differ from those of the Newtonian fluids.

5 Conclusions

The CHT on unsteady natural convection boundary layer flow of a couple stress, viscous, incompressible fluid over a vertical slender hollow cylinder has been carried out numerically. The governing equations are derived and normalised based on the length dependent effect introduced by the couple stress fluid flow where the biharmonic operator is involved. A Crank-Nicolson type of implicit method is used to solve the system of coupled governing equations together with the tridiagonal and pentadiagonal algorithms. The computations are carried out for different values of Prandtl number Pr (= 0.71, 1.0, 2.0 and 3.0) and conjugate-conduction parameter P (= 0.1, 0.5, 1.0 and 2.0).

From the present study, it is observed that the time elapsed for the velocity and temperature profiles to reach the temporal maximum increases with increasing values of Pr and P. Time required to reach the steady-state increases as Pr and P increases. It is observed that the velocity, temperature and average skin-friction coefficient of the fluid decreases with increasing values of Pr. In the vicinity of the hot wall, the velocity and temperature of the fluid decreases as P increases. It is also noticed that the steady-state values of average heat transfer rate decreases with increasing P and decreasing Pr.

Acknowledgements

The authors are thankful to the reviewers for their valuable suggestions and comments to improve the quality of the manuscript.

References

Bottemanne, F.A. (1972) 'Experimental results of pure and simultaneous heat and mass transfer by free convection about a vertical cylinder for Pr = 0.71 and Sc = 0.63', *Appl. Scientific Research*, Vol. 25, pp.372–382.

Carnahan, B., Luther, H.A. and Wilkes, J.O. (1969) *Applied Numerical Methods*, John Wiley Sons, New York.

Chang, C. (2006) 'Buoyancy and wall conduction effects on forced convection of micropolar fluid flow along a vertical slender hollow circular cylinder', *Int. J. Heat Mass Trans.*, Vol. 49, No. 25, pp.4932–4942.

Chang-Jian, C., Yau, H. and Chen, J. (2010) 'Nonlinear dynamic analysis of a hybrid squeeze-film damper-mounted rigid rotor lubricated with couple stress fluid and active control', *Applied Mathematical Modelling*, Vol. 34, No. 9, pp.2493–2507.

Char, M.I., Chen, C.K. and Cleaver, J.W. (1990) 'Conjugate forced convection heat transfer from a continuous moving flat sheet', *Int. J. Heat Fluid Flow*, Vol. 11, No. 3, pp.257–261.

Chu, H.M., Li, W.L. and Hu, S.Y. (2006) 'Effects of couple stresses on pure squeeze EHL motion of circular contacts', *J. Mech.*, Vol. 22, No. 1, pp.77–84.

Eringen, A.C. (1966) 'Theory of micropolar fluids', *J. Math. Mech.*, Vol. 16, pp.1–18.

Fujii, T. and Uehara, H. (1970) 'Laminar natural convective heat transfer from the outer surface of a vertical cylinder', *Int. J. Heat Mass Trans.*, Vol. 13, No. 3, pp.607–615.

Gdalevich, L.B. and Fertman, V.E. (1977) 'Conjugate problems of natural convection', *Inzh-Fiz. Zh.*, Vol. 33, No. 3, pp.539–547.

Kaya, A. (2011) 'Effects of buoyancy and conjugate heat transfer on non-Darcy mixed convection about a vertical slender hollow cylinder embedded in a porous medium with high porosity', *Int. J. Heat Mass Trans.*, Vol. 54, No. 4, pp.818–825.

Lee, H.R., Chen, T.S. and Armaly, B.F. (1988) Natural convection along slender vertical cylinders with variable surface temperature, *ASME J. Heat Trans.*, Vol. 110, No. 1, pp.103–108.

Lin, J. (1998) 'Squeeze film characteristics of finite journal bearings: couple stress fluid model', *Tribology International*, Vol. 31, No. 4, pp.201–207.

Minkowycz, W.J. and Sparrow, E.M. (1974) 'Local nonsimilar solutions for natural convection on a vertical cylinder', *ASME J. Heat Trans.*, Vol. 96, No. 2, pp.178–183.

Miyamoto, M., Sumikawa, J., Akiyoshi, T. and Nakamura, T. (1980) 'Effects of axial heat conduction in a vertical flat plate on free convection heat transfer', *Int. J. Heat Mass Trans.*, Vol. 23, No. 11, pp.1545–1553.

Naduvinamani, N.B. and Patil, S.B. (2009) 'Numerical solution of finite modified Reynolds equation for couple stress squeeze film lubrication of porous journal bearings', *Computers and Structures*, Vol. 87, pp.1287–1295.

Pop, I. and Na, T.Y. (2000) 'Conjugate free convection over a vertical slender hollow cylinder embedded in a porous medium', *Heat Mass Trans.*, Vol. 36, No. 5, pp.375–379.

Rani, H.P. and Kim, C.N. (2008) 'Transient free convection flow over an isothermal vertical cylinder with temperature dependent viscosity', *Korean J. Chem. Eng.*, Vol. 25, No. 1, pp.34–40.

Rani, H.P., Reddy, G.J. and Kim, C.N. (2011) 'Numerical analysis of couple stress fluid past an infinite vertical cylinder', *Engineering Applications of Computational Fluid Mechanics*, Vol. 5, No. 2, pp.159–169.

Sparrow, E.M. and Gregg, J.L. (1956) 'Laminar free convection heat transfer from the outer surface of a vertical circular cylinder', *ASME J. Heat Trans.*, Vol. 78, pp.1823–1829.

Srivastava, L.M. (1986) 'Peristaltic transport of a couple stress fluid', *Rheol Acta*, Vol. 25, No. 6, pp.638–641.

Srivastava, V.P. (2003) 'Flow of a couple stress fluid representing blood through stenotic vessels with a peripheral layer', *Indian Journal of Pure and Applied Mathematics*, Vol. 34, No. 12, pp.1727–1740.

Stokes, V.K. (1966) 'Couple stress in fluids', *Physics Fluids*, Vol. 9, No. 9, pp.1709–1715.

Stokes, V.K. (1984) *Theories of Fluids with Microstructure*, Springer-Verlag, New York, Tokyo.

Umavathi, J.C. and Malashetty, M.S. (1999) 'Oberbeck convection flow of a couple stress fluid through a vertical porous stratum', *Int. J. Non-Linear Mech.*, Vol. 34, No. 6, pp.1037–1045.

Von Rosenberg, D.U. (1969) *Rosenberg, Methods for the Numerical Solution of Partial Differential Equations*, American Elsevier Publishing Company, New York.

Nomenclature

$\overline{C_f}$	Dimensionless average skin-friction coefficient
C_f	Dimensionless local skin-friction coefficient
g	Acceleration due to gravity
Gr	Grashof number
k_f, k_s	Thermal conductivity of the fluid and the solid cylinder, respectively
l	Length of the cylinder
$\overline{Nu}$	Dimensionless average Nusselt number
Nu_X	Dimensionless local Nusselt number
P	Conjugate-conduction parameter
Pr	Prandtl number
r	Radial coordinate
r_i, r_0	Inner and outer radii of the hollow cylinder, respectively
R	Dimensionless radial coordinate
t'	Time
t	Dimensionless time
${T_0}'$	Temperature at the inside surface of the cylinder
${T_s}'$	Solid temperature
T'	Temperature of the fluid
T	Dimensionless temperature of the fluid
u, v	Velocity components in x, r directions, respectively
U, V	Dimensionless velocity components in X, R directions, respectively
x	Axial coordinate
X	Dimensionless axial coordinate

Greek letters	
α	Thermal diffusivity
β	Volumetric coefficient of thermal expansion
η	Material constant
ρ	Density
μ	Viscosity of the fluid
ν	Kinematic viscosity
Subscripts	
w	Conditions on the wall
∞	Free stream conditions
Superscript	
k	Time step level